A Reversible Residual Network-Aided Canonical Correlation Analysis to Fault Detection and Diagnosis in Electrical Drive Systems

Shenquan Wang (王申全), Yunfei Ju (鞠云飞), *Graduate Student Member, IEEE*, Caixin Fu (付彩欣), Pu Xie (谢普), and Chao Cheng (程超), *Member, IEEE*

***Abstract*— To ensure the safety of electrical drive systems, fault detection and diagnosis (FDD) has become an active approach over the past two decades. Multivariate analysis is a popular method in FDD, among which canonical correlation analysis (CCA) has been widely applied and studied. However, most CCA-based fault detection (FD) methods assume that the signal is Gaussian and that there is a linear relationship between the variables. Since the electrical drive systems are nonlinear, these CCA-based FD methods are not optimal. With the help of the reversible residual network, this article proposes a reversible residual network-aided CCA (RRNCCA) for fault diagnosis. The main work is as follows: 1) the objective function of RRNCCA is reformulated; 2) RRNCCA-based FDD is first designed for electrical drive systems; and 3) through the difference in FD results, fault diagnosis is directly achieved. The effectiveness of the proposed method is verified via an electrical drive system.**

***Index Terms*— Canonical correlation analysis (CCA), electrical drive systems, fault detection and diagnosis (FDD), reversible residual network.**

I. Introduction

THE high safety requirements have led to the development of fault detection and diagnosis (FDD) in electrical drive systems [1]. The electrical drive systems install a large number of sensors for safe operation. If the sensors break down, the values collected by the sensors will deviate from their expected values [2]. The wrong information will affect the control of the electrical drive system or even lead to an accident in the system [3]. Therefore, it is necessary to improve the safety of the electrical drive system through sensor FDD.

Nowadays, the methods are usually adopted to detect faults in electrical drive systems: model-based and data-driven [4], [5], [6], [7], [8], [9], [10]. Most model-based fault detection (FD) methods require rigorous physical and mathematical models, which pose grievous limitations on practical applications [11]. Therefore, the model-based FD applications are still rare in real-world electrical drive systems.

The data-driven FD methods will show superior advantages when an accurate mathematical model or expert knowledge about traction systems is absent. Multivariate statistical analysis is the most commonly used approach in data-based FDD methods [12]. The least squares [13], principal component analysis [14], and independent component analysis are classic methods for multivariate statistical analysis. In addition, the canonical correlation analysis (CCA) is born by considering the correlation between two datasets, which also belongs to the multivariate statistical analysis. Researchers have designed many CCA variants for FDD [15], [16], [17].

By analyzing the values collected by the sensor, the CCA can find two sets of linear bases to obtain the maximum correlation of features in the projected space [18]. A modified CCA scheme is developed for finding a proper decision threshold in non-Gaussian variables [19]. Chen et al. [16] utilize CCA to obtain the residual error by considering the correlation between each fault characterization index to realize fast FD. In addition, combined with broad learning, a fast CCA-based FD method is proposed [20]. The CCA-based linear FD achieves substantial results.

Among various nonlinear schemes, artificial neural network-based versions are the most popular [21]. For example, the deep CCA is extended for FD in nonlinear systems [22]. To FD in nonlinear systems, neural network-aided CCA scheme is proposed [15]. A deep neural network-aided CCA method is proposed for the FD of nonlinear dynamical systems [17].

The existing neural network-based CCA method can extract the maximum correlation of two datasets very well [15]. However, the problem remains, namely the performance of the FD in electrical drive systems. Although neural network-aided CCA uses the FD ability of test statistics to perform FDD tasks, it does not have a corresponding theory to push the process. For example, the two projections generation by neural

Manuscript received 14 October 2023; revised 14 December 2023; accepted 16 December 2023. Date of publication 2 January 2024; date of current version 29 February 2024. This work was supported in part by the National Natural Science Foundation of China under Grant 62372063 and Grant 62273058, in part by the Department of Science and Technology of Jilin Province under Grant 20230508112RC and Grant 20230508043RC, and in part by the Changchun Science and Technology Bureau under Grant 21GD05. The Associate Editor coordinating the review process was Dr. Hongtian Chen. *(Corresponding author: Chao Cheng.)*

Shenquan Wang is with the School of Electrical and Electronical Engineering, Changchun University of Technology, Changchun 130012, China (e-mail: shenquanwang@126.com).

Yunfei Ju and Caixin Fu are with the School of Mechanical and Electrical Engineering, Changchun University of Technology, Changchun 130012, China (e-mail: juyunfei1998@163.com; fucaixin8932@163.com).

Pu Xie is with the Department of Aeronautics and Astronautics, Stanford University, Stanford, CA 94305 USA (e-mail: xiepu@stanford.edu).

Chao Cheng is with the School of Computer Science and Engineering, Changchun University of Technology, Changchun 130012, China (e-mail: chengx415@163.com).

Digital Object Identifier 10.1109/TIM.2023.3348900

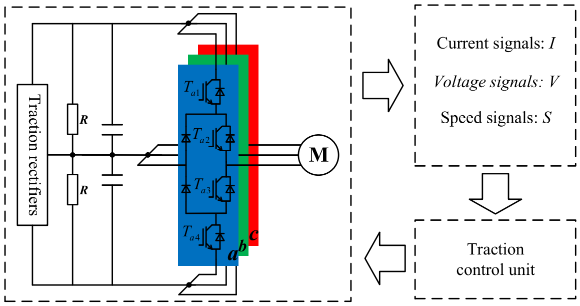

Fig. 1. Electrical drive system.

network-assisted CCA may attenuate the impact caused by the fault. It will affect the FD ability of the test statistic, which in turn affects the fault diagnosis.

These observations prompted the design of a reversible residual network-aided CCA (RRNCCA) framework to implement FDD in electrical drive systems.

1) Unlike other neural network CCA methods, in this article, CCA is aided by the reversible residual neural network (RRN) to extract the correlation between nonlinear variables. A reversible loop is constructed so that the nonlinear projection of two data has a reversible mapping while ensuring maximum correlation.
2) Four sets of residual generators are defined based on the RRNCCA method. Test statistics are designed from residual generators to improve the FD performance of electrical drive systems.
3) The FDD is achieved through the difference in FD results.

The rest of this article is organized as follows. Section II introduces the signal-based electrical drive system model, RRN, CCA, and the objective of this work. In Section III, a version of RRNCCA is developed, and the FDD performance is proven. Section IV illustrates the effectiveness of the RRNCCA-based method via the electrical drive system model. This article is concluded in Section V.

II. Preliminaries and Objectives

This section presents the basics of electrical drive systems and RRN. The CCA-based residual information is derived, and the objectives of this study are formulated.

A. System Model

The nonlinear system model is as follows [23]:

$$\begin{cases} x(k+1) = f_x(x(k), u(k), w(k)) \\ y(k) = g_x(x(k), u(k), v(k)) \end{cases} \tag{1}$$

where $f_x(\cdot)$ and $g_x(\cdot)$ are nonlinear mappings; $u(k) \in R^{k_u}$, $y(k) \in R^{k_y}$, and $x(k) \in R^{k_x}$ are input, output, and state vectors of the system, respectively. Without losing generality, there are assumptions $w \sim N(0, \Sigma_w)$ and $v \sim N(0, \Sigma_v)$. Fig. 1 is a sketch of the electrical drive system.

With the continuous development of data-driven technology, a signal-based form of representation has emerged as follows [12]:

$$z(k) = \left[u^T(k), y^T(k)\right]^T. \tag{2}$$

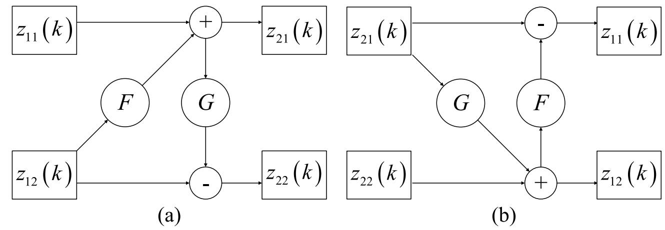

Fig. 2. RRN framework.

$Z = [z(1), z(2), \ldots, z(n)] \in R^{(k_u+k_y)\times n}$ is the system dataset. n is the total number of sensor acquisitions. It is obtained directly from sensor acquisition and does not require mathematical modeling. If the system is affected by faults, the data collected by the sensor will change somewhat [24]. Therefore, the data with fault information is

$$z^f(k) = \begin{bmatrix} z_1^f(k) \\ z_2(k) \end{bmatrix}, \quad z^f(k) = \begin{bmatrix} z_1(k) \\ z_2^f(k) \end{bmatrix}, \; z^f(k) = \begin{bmatrix} z_1^f(k) \\ z_2^f(k) \end{bmatrix}$$
$$z_1^f(k) = z_1(k) + f(k), z_2^f(k) = z_2(k) + f(k) \tag{3}$$

where $f(k)$ is the amplitude of fault. It provides a clear faults statement for follow-up work.

B. RRN

The residual function is $x_2 = x_1 + f_R(x_1)$. x_1 and x_2 are vectors/matrices of the same dimension; $f_R(\cdot)$ is linear/nonlinear mappings. The RRN is an extended form of residual network [25]. The RRN is defined as

$$\begin{aligned} &\text{forward}\begin{cases} z_{11}(k) + F(z_{12}(k)) = z_{21}(k) \\ z_{12}(k) - G(z_{21}(k)) = z_{22}(k) \end{cases} \\ &\text{reverse}\begin{cases} z_{21}(k) - F(z_{12}(k)) = z_{11}(k) \\ z_{22}(k) + G(z_{21}(k)) = z_{12}(k) \end{cases} \end{aligned} \tag{4}$$

where $z_1(k) = [z_{11}^T(k), z_{12}^T(k)]^T$; $z_{11}(k) \in R^{k_{z_1}}$; $z_{12}(k) \in R^{k_{z_2}}$; $z_2(k) = [z_{21}^T(k), z_{22}^T(k)]^T$; $z_{21}(k) \in R^{k_{z_1}}$; $z_{22}(k) \in R^{k_{z_2}}$. F and G are linear/nonlinear mappings. Fig. 2 is the RRN framework. According to the aforementioned statements, the neural network of F and G cascades is defined as

$$\theta \triangleq \begin{bmatrix} \begin{bmatrix} I & F \end{bmatrix} \\ \begin{bmatrix} I & -G \end{bmatrix} \circ \begin{bmatrix} 0 & I \\ I & F \end{bmatrix} \end{bmatrix}, \quad \theta^{-1} \triangleq \begin{bmatrix} \begin{bmatrix} -F & I \end{bmatrix} \circ \begin{bmatrix} G & I \\ I & 0 \end{bmatrix} \\ \begin{bmatrix} G & I \end{bmatrix} \end{bmatrix}$$

where $\circ$ is the cascade connection of two operators. See Appendix A for a detailed derivation process. θ stands for

$$\begin{aligned} &\theta : z_1(k) \to z_2(k), \quad \theta^{-1} : z_2(k) \to z_1(k) \\ &\theta z_1(k) = z_2(k), \quad \theta^{-1} z_2(k) = z_1(k). \end{aligned} \tag{5}$$

C. CCA-Based Residuals and Formulate Objectives

The process variables $z_1(k)$ and $z_2(k)$ obey

$$z(k) = \begin{bmatrix} z_1(k) \\ z_2(k) \end{bmatrix} \sim N\left(\begin{bmatrix} \mu_{z_1} \\ \mu_{z_2} \end{bmatrix}, \begin{bmatrix} \Sigma_{z_1} & \Sigma_{z_1 z_2} \\ \Sigma_{z_1 z_2}^T & \Sigma_{z_2} \end{bmatrix}\right) \tag{6}$$

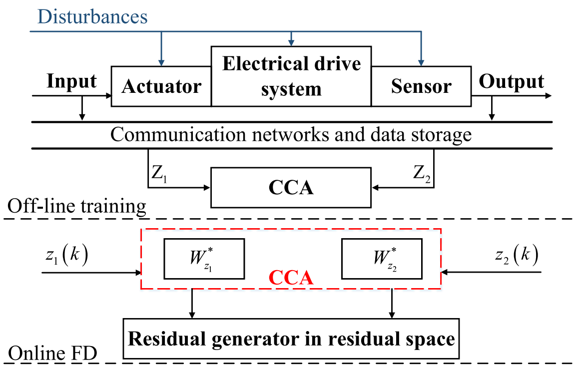

Fig. 3. Sketch of the CCA-aided FD method.

where μ_{z_1} and μ_{z_2} are mean; Σ_{z_1}, $\Sigma_{z_1z_2}$, and Σ_{z_2} are covariance matrices. The generalized objective function based on CCA defines $R_{\text{CCA}} : R^{k_{z_1}+k_{z_2}} \times R^{k_{z_1}+k_{z_2}} \to R$ as [26]

$$R_{\text{CCA}} = k_{z_1} + k_{z_2} - \operatorname{Tr}\left(\left|\Sigma_{z_1}^{-\frac{1}{2}}\Sigma_{z_1z_2}\Sigma_{z_2}^{-\frac{1}{2}}\right|\right) \tag{7}$$

where z_1 and z_2 are mean centered; $|\cdot|$ represents the absolute value operator; $\operatorname{Tr}(\cdot)$ is a trace operator.

The singular value decomposition of (7) is decomposed into $R_{\text{CCA}} = S\Sigma D$, where $S = [s_1, \ldots, s_{k_{z_1}+k_{z_2}}]$; $\Sigma = \begin{bmatrix} \Sigma_{k_d} & 0 \\ 0 & 0 \end{bmatrix}$; $D = [d_1, \ldots, d_{k_{z_1}+k_{z_2}}]^T$; k_d is the number of principal components; $\sum_{k_d} = \operatorname{diag}(\rho_1, \ldots, \rho_{k_d})$; $1 \geq \rho_1 \geq \cdots \geq \rho_{k_d} \geq 0$ are canonical correlation coefficients [27]. The canonical vectors are defined as

$$W_{z_1} = \Sigma_{z_1}^{-\frac{1}{2}} S_r, \;\; W_{z_2} = \Sigma_{z_2}^{-\frac{1}{2}} D_r \tag{8}$$

where r is the number of nonzero singular values; $r = \operatorname{rank}(\Sigma) \leq \min\{k_{z_1} + k_{z_2}\}$; S_r and D_r are the first r columns in the corresponding matrices.

Therefore, the optimization problem is defined as

$$\begin{aligned}\left(W_{z_1}^*, W_{z_2}^*\right) &= \arg\max W_{z_1}^T \Sigma_{z_1z_2} W_{z_2} \\ &= \arg\min \operatorname{CCA}\left(z_1, z_2; W_{z_1}, W_{z_2}\right) \\ \text{s.t. } W_{z_1}^T \Sigma_{z_1} W_{z_1} &= 1, \;\; W_{z_2}^T \Sigma_{z_2} W_{z_2} = 1.\end{aligned} \tag{9}$$

Through Lagrangian multipliers, (9) is rewritten as

$$\begin{aligned}L\left(W_{z_1}, W_{z_2}, \lambda_{z_1}, \lambda_{z_2}\right) = W_{z_1}^T \Sigma_{z_1z_2} W_{z_2} &+ \frac{\lambda_{z_1}}{2}\left(W_{z_1}^T \Sigma_{z_1} W_{z_1} - 1\right) \\ &+ \frac{\lambda_{z_2}}{2}\left(W_{z_2}^T \Sigma_{z_2} W_{z_2} - 1\right).\end{aligned} \tag{10}$$

Through (10), the residual signal is defined as [16]

$$\begin{aligned}\gamma_1(k) &= \left[W_{z_1}^* \;\; -\Sigma W_{z_2}^*\right]\left[z_1^T(k), z_2^T(k)\right]^T \\ \gamma_2(k) &= \left[-\Sigma^T W_{z_1}^* \;\; W_{z_2}^*\right]\left[z_1^T(k), z_2^T(k)\right]^T.\end{aligned} \tag{11}$$

Fig. 3 is a CCA-aided FD method. Here, $Z = [Z_1^T, Z_2^T]^T$; $Z_1 = [z_1(1), z_1(2), \ldots, z_1(n)] \in R^{(k_{z_1}+k_{z_2})\times n}$; $Z_2 = [z_2(1), z_2(2), \ldots, z_2(n)] \in R^{(k_{z_1}+k_{z_2})\times n}$. For the FD ability of $\gamma_1(k)$ and $\gamma_2(k)$, the T^2-test statistic is defined as

$$\begin{aligned}T^2(\gamma_1(k)) &= \gamma_1^T(k)\Sigma_{\gamma_1}^{-1}\gamma_1(k) \\ T^2(\gamma_2(k)) &= \gamma_2^T(k)\Sigma_{\gamma_2}^{-1}\gamma_2(k)\end{aligned} \tag{12}$$

where $\Sigma_{\gamma_1}^{-1}$ and $\Sigma_{\gamma_2}^{-1}$ are covariance matrices.

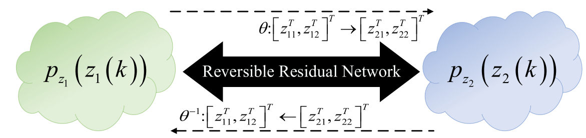

Fig. 4. Probabilistic model of RRN.

In an ideal situation, if there is no-fault in the system, then

$$T^2(\gamma_1(k)) \leq T_{\text{th}_1} \text{ and } T^2(\gamma_2(k)) \leq T_{\text{th}_2} \tag{13}$$

where T_{th_1} and T_{th_2} are threshold. If system fails, there is

$$T^2\left(\gamma_1^f(k)\right) > T_{\text{th}_1} \text{ or } T^2\left(\gamma_2^f(k)\right) > T_{\text{th}_2} \tag{14}$$

where $\gamma_1^f(k)$ and $\gamma_2^f(k)$ are residual signals with faults. Based on the understanding of CCA, the objectives are formulated as follows.

1) The RRNCCA framework is designed to implement reversible nonlinear mapping.
2) A residual generator based on RRNCCA is proposed.
3) The T^2 test statistic is designed with four sets of residual signals to achieve the FDD of the electrical drive systems.

III. RRNCCA-Based FDD

This section presents the RRNCCA method to find reversible projections. Based on the proposed RRNCCA approach to achieve FDD.

A. RRNCCA Framework

The process data $z(k)$ of the system is given. Combined with (5), the probabilistic model obtained is

$$\log\left(p_{z_1}(z_1(k))\right) = \log\left(p_{z_2}(\theta z_1(k))\right) + \log\left(\left|\det\left(\frac{\partial\theta z_1(k)}{\partial z_1{}^T(k)}\right)\right|\right) \tag{15}$$

where $z_1{-}p_{z_1}(\cdot)$ and $z_2{-}p_{z_2}(\cdot)$ are probability distributions; $[(\partial\theta z_1(k))/(\partial z_1^T(k))]$ is the Jacobian of θ at $z_1(k)$. The last term of (15) in RRN is [28]

$$\det\left(\frac{\partial\theta z_1(k)}{\partial z_1{}^T(k)}\right) = 1. \tag{16}$$

See Appendix B for a detailed derivation process. Fig. 4 is a probabilistic model of RRN. The RRN algorithm is given as Algorithms 1 and 2. The activations $[z_{21}(k), z_{22}(k)]$ and their total derivatives $[\bar{z}_{21}(k), \bar{z}_{22}(k)]$ are given to compute the inputs $[z_{11}(k), z_{12}(k)]$. The total derivatives are $[\bar{z}_{11}(k), \bar{z}_{12}(k)]$. The total derivatives are $(\bar{w}_F, \bar{w}_G)$ for any parameters associated with F and G. For this model, forward and backward reasoning are equally effective. There is a one-to-one correspondence between input and output [29]. The information is not lost [25].

CCA is finding two sets of mappings to maximize correlation [30]. Combined with (9), the loss function is

$$L_{\text{CCA}} = \operatorname{CCA}\left(z_1(k), \theta_C z_1(k); W_{z_1}^*, W_{z_2}^*\right) \tag{17}$$

Algorithm 1 RRN Block Forward

Load $\left((z_{11}(k), z_{12}(k)), \left(\bar{z}_{11}(k), \bar{z}_{12}(k)\right)\right)$;

$z_{21}(k) \leftarrow z_{11}(k) + F(z_{12}(k))$;

$z_{22}(k) \leftarrow z_{12}(k) - G(z_{21}(k))$;

$\bar{z}_{22}(k) \leftarrow \bar{z}_{12}(k) - \left(\frac{\partial F}{\partial z_{22}(k)}\right)^T \bar{z}_{11}(k)$

$\bar{z}_{21}(k) \leftarrow \bar{z}_{11}(k) + \left(\frac{\partial G}{\partial z_{21}(k)}\right)^T \bar{z}_{22}(k)$;

$\bar{w}_F \leftarrow \left(\frac{\partial F}{\partial w_F}\right)^T \bar{z}_{11}(k)$;

$\bar{w}_G \leftarrow \left(\frac{\partial G}{\partial w_G}\right)^T \bar{z}_{22}(k)$;

Return $\left((z_{21}(k), z_{22}(k)), \left(\bar{z}_{21}(k), \bar{z}_{22}(k)\right), \left(\bar{w}_F, \bar{w}_G\right)\right)$.

Algorithm 2 RRN Block Backward

Load $\left((z_{21}(k), z_{22}(k)), \left(\bar{z}_{21}(k), \bar{z}_{22}(k)\right)\right)$;

$z_{12}(k) \leftarrow z_{22}(k) + G(z_{21}(k))$;

$z_{11}(k) \leftarrow z_{21}(k) - F(z_{12}(k))$;

$\bar{z}_{11}(k) \leftarrow \bar{z}_{21}(k) - \left(\frac{\partial G}{\partial z_{11}(k)}\right)^T \bar{z}_{22}(k)$;

$\bar{z}_{12}(k) \leftarrow \bar{z}_{22}(k) + \left(\frac{\partial F}{\partial z_{12}(k)}\right)^T \bar{z}_{11}(k)$;

$\bar{w}_F \leftarrow \left(\frac{\partial F}{\partial w_F}\right)^T \bar{z}_{11}(k)$;

$\bar{w}_G \leftarrow \left(\frac{\partial G}{\partial w_G}\right)^T \bar{z}_{22}(k)$;

Return $\left((z_{11}(k), z_{12}(k)), \left(\bar{z}_{11}(k), \bar{z}_{12}(k)\right), \left(\bar{w}_F, \bar{w}_G\right)\right)$.

where θ_C is nonlinear mapping. The solution of θ_C is

$$\theta_C^* = \arg\min L_{\mathrm{CCA}}. \tag{18}$$

Combining (11), (12), and (17), (18) is equivalent to

$$\theta_C^* = \arg\min T^2(\gamma_1(k)) \text{ or } \theta_C^* = \arg\min T^2(\gamma_2(k)). \tag{19}$$

Then, the Cauchy–Schwarz inequality directly results in

$$\begin{aligned} &\arg\min T^2(\gamma_1(k)) \\ &\quad= \arg\min\left\| \Sigma_{\gamma_1}^{-\frac{1}{2}} \left(W_{z_1}^* z_1(k) - \Sigma W_{z_2}^* \circ \theta_C z_1(k)\right)\right\|_2^2 \\ &\quad= \arg\min\left\| W_{z_1}^* z_1(k) - \Sigma W_{z_2}^* \circ \theta_C z_1(k)\right\|_2^2 \end{aligned} \tag{20}$$

where $\Sigma_{\gamma_1}^{-(1/2)}$ and $W_{z_1}^* z_1(k) - \Sigma W_{z_2}^* \circ \theta_C z_1(k)$ are linearly dependent [15]. In the same way

$$\begin{aligned} &\arg\min T^2(\gamma_2(k)) \\ &\quad= \arg\min\left\| W_{z_2}^* \circ \theta_C z_1(k) - \Sigma^T W_{z_1}^* z_1(k)\right\|_2^2. \end{aligned} \tag{21}$$

By analyzing relationship among (11), (20), and (21), one has

$$\begin{aligned} &\left\| W_{z_1}^* z_1(k) - \Sigma W_{z_2}^* z_2(k)\right\|_2^2 \\ &\quad= \min\left\| W_{z_1}^* z_1(k) - \Sigma W_{z_2}^* \circ \theta_C z_1(k)\right\|_2^2 \\ &\left\| W_{z_2}^* z_2(k) - \Sigma^T W_{z_1}^* z_1(k)\right\|_2^2 \\ &\quad= \min\left\| W_{z_2}^* \circ \theta_C z_1(k) - \Sigma^T W_{z_1}^* z_1(k)\right\|_2^2. \end{aligned} \tag{22}$$

According to (22), the final solution is

$$\begin{aligned} \theta_{\mathrm{RC}}^* &= \arg\min L_{\mathrm{RR-CCA}} \\ L_{\mathrm{RR-CCA}} &= \|z_2(k) - \theta_{\mathrm{RC}} z_1(k)\|_2^2 \\ &\quad \text{s.t. } (9). \end{aligned} \tag{23}$$

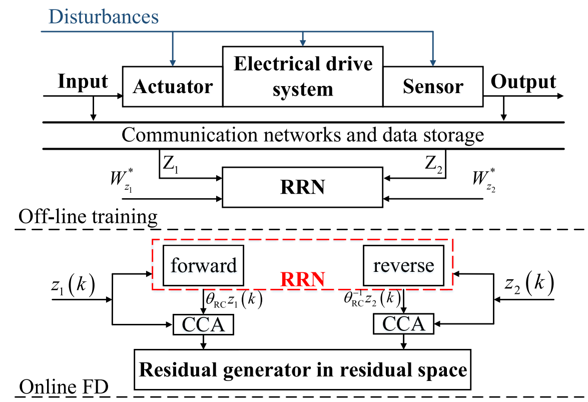

Fig. 5. Residual generator of RRNCCA.

To achieve FD, the residuals are defined as

$$\begin{aligned} \gamma_{11}(k) &= W_{z_1}^* z_1(k) - \Sigma W_{z_2}^* \circ \theta_{\mathrm{RC}} z_1(k) \\ \gamma_{12}(k) &= W_{z_2}^* \circ \theta_{\mathrm{RC}} z_1(k) - \Sigma^T W_{z_1}^* z_1(k). \end{aligned} \tag{24}$$

Since θ_{RC} is reversible, the inverse residuals are defined as

$$\begin{aligned} \gamma_{21}(k) &= W_{z_1}^* \circ \theta_{\mathrm{RC}}^{-1} z_2(k) - \Sigma W_{z_2}^* z_2(k) \\ \gamma_{22}(k) &= W_{z_2}^* z_2(k) - \Sigma^T W_{z_1}^* \circ \theta_{\mathrm{RC}}^{-1} z_2(k). \end{aligned} \tag{25}$$

The residual generator of RRNCCA is shown in Fig. 5.

B. FDD

Considering the system including faults, the residual generator of RRNCCA has three forms. In Section III-B, three forms of RRNCCA-based residual generators are described in detail. Let be the system failure to cause $z_1(k)$ abnormal. The residual signal is

$$\begin{aligned} \gamma_{11}^f(k) &= W_{z_1}^* (z_1(k) + f(k)) - \Sigma W_{z_2}^* \circ \theta_{\mathrm{RC}}(z_1(k) + f(k)) \\ \gamma_{12}^f(k) &= W_{z_2}^* \circ \theta_{\mathrm{RC}}(z_1(k) + f(k)) - \Sigma^T W_{z_1}^* (z_1(k) + f(k)) \\ \gamma_{21}^f(k) &= W_{z_1}^* \circ \theta_{\mathrm{RC}}^{-1} z_2(k) - \Sigma W_{z_2}^* z_2(k) \\ \gamma_{22}^f(k) &= W_{z_2}^* z_2(k) - \Sigma^T W_{z_1}^* \circ \theta_{\mathrm{RC}}^{-1} z_2(k). \end{aligned} \tag{26}$$

The Taylor expansion of $\theta_{\mathrm{RC}}(z_1(k) + f(k))$ is

$$\begin{aligned} \theta_{\mathrm{RC}}(z_1(k) + f(k)) &= \theta_{\mathrm{RC}} z_1(k) + \nabla\theta_{\mathrm{RC}}(z_1(k)) f(k) \\ &\quad + \frac{1}{2} f^T(k) H(\theta_{\mathrm{RC}} z_1(k)) f(k) + \cdots \end{aligned} \tag{27}$$

where $\nabla\theta_{\mathrm{RC}}(z_1(k))$ and $H(\theta_{\mathrm{RC}} z_1(k))$ represent the Jacobian and Hessian matrix of θ_{RC} at $z_1(k)$, respectively [24]. The expansion term above the second order of (27) is ignored. Equation (27) is substituted into (Section III-B) to obtain

$$\begin{aligned} \gamma_{11}^f(k) &= W_{z_1}^* z_1(k) - \Sigma W_{z_2}^* \circ \theta_{\mathrm{RC}} z_1(k) \\ &\quad + W_{z_1}^* f(k) - \Sigma W_{z_2}^* \circ \nabla\theta_{\mathrm{RC}}(z_1(k)) f(k) \\ &\quad - \Sigma W_{z_2}^* \circ \frac{1}{2} f^T(k) H(\theta_{\mathrm{RC}} z_1(k)) f(k). \end{aligned} \tag{28}$$

Alternatively, if θ_{RC} is known, there is

$$\begin{aligned} & W_{z_1}^* f(k) - \Sigma W_{z_2}^* \circ \left(\nabla\theta_{\mathrm{RC}}^* z_1(k)\right) f(k) \\ &\quad = \left(W_{z_1}^* - \Sigma W_{z_2}^*\right) f(k) \\ &\quad = C f(k) \\ & \text{s.t. } \nabla\theta_{\mathrm{RC}}^* z_1(k) = \frac{\partial \theta_{\mathrm{RC}}^* z_1(k)}{\partial \theta_{\mathrm{RC}}^*} + \frac{\partial \theta_{\mathrm{RC}}^* z_1(k)}{\partial z_1(k)} = I \end{aligned} \tag{29}$$

where $C \triangleq (W_{z_1}^* - \Sigma W_{z_2}^*)$. The residual signal with faults is

$$\begin{aligned} \gamma_{11}^f(k) &= W_{z_1}^* z_1(k) - \Sigma W_{z_2}^* \circ \theta_{\mathrm{RC}} z_1(k) + C f(k) \\ &\quad - \Sigma W_{z_2}^* \circ \left(\frac{1}{2} f^T(k) H(\theta_{\mathrm{RC}} z_1(k)) f(k)\right) \\ &= \gamma_{11}(k) + f_{\mathrm{term}}^{11}(k) \end{aligned} \tag{30}$$

where $f_{\mathrm{term}}^{11}(k) \triangleq C f(k) - \Sigma W_{z_2}^* \circ ((1/2) f^T(k) H(\theta_{\mathrm{RC}} z_1(k))$ $f(k))$. Similarly, according to (30), $\gamma_{12}^f(k)$, $\gamma_{21}^f(k)$, and $\gamma_{22}^f(k)$ can obtain the similar form. For a system with $z_{11}(k)$ fault, the T^2 test statistic can be denoted as

$$\begin{aligned} & T^2\left(\gamma_{11}^f(k)\right) \\ &\quad = \left(\gamma_{11}(k) + f_{\mathrm{term}}^{11}(k)\right)^T \Sigma_{\gamma_{11}}^{-1}\left(\gamma_{11}(k) + f_{\mathrm{term}}^{11}(k)\right). \end{aligned} \tag{31}$$

In general, the unknown fault is uncorrelated with both $z_1(k)$ and $z_2(k)$, resulting in

$$\begin{aligned} & E\left[T^2\left(\gamma_{11}^f(k)\right)\right] \\ &= E\left[\left(\gamma_{11}(k) + f_{\mathrm{term}}^{11}(k)\right)^T \Sigma_{\gamma_{11}}^{-1}\left(\gamma_{11}(k) + f_{\mathrm{term}}^{11}(k)\right)\right] \\ &= T^2(\gamma_{11}(k)) + E\left[\left(f_{\mathrm{term}}^{11}(k)\right)^T \Sigma_{\gamma_{11}}^{-1} f_{\mathrm{term}}^{11}(k)\right] \\ &= T^2(\gamma_{11}(k)) \\ &\quad + \left(f_{\mathrm{term}}^{11}(k)\right)^T \Sigma_{\gamma_{11}}^{-\frac{1}{2}} \mathrm{diag}\left(\frac{1}{1-\rho_1^2}, \ldots, \frac{1}{1-\rho_{k_d}^2}\right) \Sigma_{\gamma_{11}}^{-\frac{1}{2}} f_{\mathrm{term}}^{11}(k) \end{aligned} \tag{32}$$

where $E[\cdot]$ is expectation; Fig. 6 shows the flowchart of FDD.

If there is a fault in the $z_1(k)$ signal, then

$$\begin{aligned} & T^2\left(\gamma_{11}^f(k)\right) > T_{\mathrm{th}_{11}}, \quad T^2\left(\gamma_{12}^f(k)\right) > T_{\mathrm{th}_{12}} \\ & T^2\left(\gamma_{21}^f(k)\right) \le T_{\mathrm{th}_{21}}, \quad T^2\left(\gamma_{22}^f(k)\right) \le T_{\mathrm{th}_{22}}. \end{aligned} \tag{33}$$

If there is a fault in the $z_2(k)$ signal, then

$$\begin{aligned} & T^2\left(\gamma_{11}^f(k)\right) \le T_{\mathrm{th}_{11}}, \quad T^2\left(\gamma_{12}^f(k)\right) \le T_{\mathrm{th}_{12}} \\ & T^2\left(\gamma_{21}^f(k)\right) > T_{\mathrm{th}_{21}}, \quad T^2\left(\gamma_{22}^f(k)\right) > T_{\mathrm{th}_{22}}. \end{aligned} \tag{34}$$

If the $z_1(k)$ and $z_2(k)$ signals are fault, then

$$\begin{aligned} & T^2\left(\gamma_{11}^f(k)\right) > T_{\mathrm{th}_{11}}, \quad T^2\left(\gamma_{12}^f(k)\right) > T_{\mathrm{th}_{12}} \\ & T^2\left(\gamma_{21}^f(k)\right) > T_{\mathrm{th}_{21}}, \quad T^2\left(\gamma_{22}^f(k)\right) > T_{\mathrm{th}_{22}}. \end{aligned} \tag{35}$$

The RRNCCA-based residual generator can diagnose where fault signal occurs. The signal fluctuation of z_1 or z_2 is fault.

The process of converting the residual signal into a single value using the T^2 test statistic is called model evaluation. The residual signal that does not contain fault information cannot be greater than one constant. This constant is the threshold for evaluating the model. Since the system is nonlinear, the threshold no longer obeys the chi-square distribution. The threshold is defined as

$$T_{\mathrm{th}} = \max T_\gamma^2 \tag{36}$$

where $T_\gamma^2 = [T^2(\gamma(1)), T^2(\gamma(2)), \ldots, T^2(\gamma(n))]$.

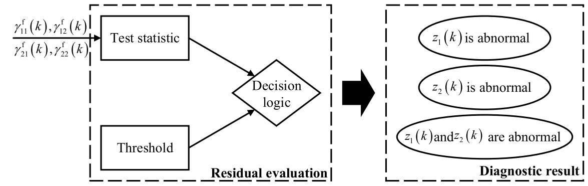

Fig. 6. FDD of RRNCCA-based residual generator.

Algorithm 3 RRNCCA-Based FDD: Offline Training

1: Load data;
2: Define $\left(W_{z_1}^*, W_{z_2}^*\right)$ via; (9);
3: Construct neural network whose loss function is defined in (23);
4: Obtain $(G^*, F^*) \to \theta_{\mathrm{RC}}^*$;
5: Generate residual signals based on (24) and (25);
6: Calculate threshold via (36).

Algorithm 4 RRNCCA-Based FDD: Online Application

1: Read online sigal $Z^{\mathrm{on}} = \begin{bmatrix} z_1^{\mathrm{on}} \\ z_2^{\mathrm{on}} \end{bmatrix}$;
2: Calculate four residual signals in real time;
3: Generate $T^2\left(\gamma_{11}^{\mathrm{on}}\right)$, $T^2\left(\gamma_{12}^{\mathrm{on}}\right)$, $T^2\left(\gamma_{21}^{\mathrm{on}}\right)$, and $T^2\left(\gamma_{22}^{\mathrm{on}}\right)$ via (12);
4: Declare FD by

$$\begin{cases} \begin{cases} T^2\left(\gamma_{11}^{\mathrm{on}}\right) \le T_{\mathrm{th}_{11}} \\ T^2\left(\gamma_{12}^{\mathrm{on}}\right) \le T_{\mathrm{th}_{12}} \\ T^2\left(\gamma_{21}^{\mathrm{on}}\right) \le T_{\mathrm{th}_{21}} \\ T^2\left(\gamma_{22}^{\mathrm{on}}\right) \le T_{\mathrm{th}_{22}} \end{cases} \Rightarrow \text{fault}-\text{free}, \\ \text{otherwise} \Rightarrow \text{fault alarm}; \end{cases}$$

5: Go back to step 1 if the system is fault-free;
6: Diagnose faults via (33), (34), and (35);
7: Go back to step 1.

C. FDD Strategy

With the above description and analysis, RRNCCA method steps are divided into two parts. Algorithms 3 and 4 are designed for offline training and online FDD, respectively.

IV. Experimental Verifications

In this section, a nonlinear electrical drive system is adopted to demonstrate the effectiveness of the proposed RRNCCA-based FDD method, followed by some discussions.

A. Electrical Drive System

This article focuses on electrical traction systems with a vector control strategy. The operation of a permanent magnet

TABLE I
PARAMETERS FOR ELECTRICAL DRIVE SYSTEM

Symbol	Quantity	Value (Unit)
J_m	moment of inertia	$0.425 \times 10^{-3}(\mathrm{kg} \cdot \mathrm{m}^2)$
p	pole pairs	4
R_a	resistance of motor coil	$0.985\,(\Omega)$
L_a	inductance of motor coil	$2.96 \times 10^{-3}(\mathrm{H})$
O_a	magnet flux	$8.1 \times 10^{-2}(\mathrm{Wb})$
T_e	electromagnetic torque	$2.43\,(\mathrm{N} \cdot \mathrm{m})$
D_m	viscosity friction coefficient	1×10^{-4}
T_L	load torque	$3.645\,(\mathrm{N} \cdot \mathrm{m})$
T_s	sampling time	$1 \times 10^{-4}\,(\mathrm{s})$

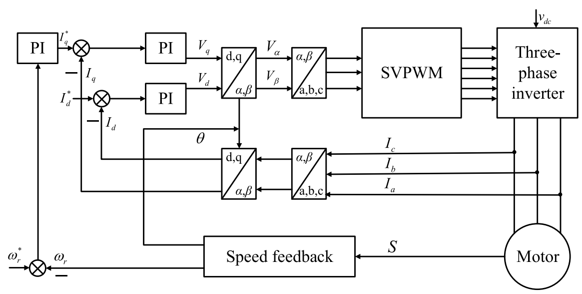

Fig. 7. Structure diagram of electrical drive system with vector control strategy.

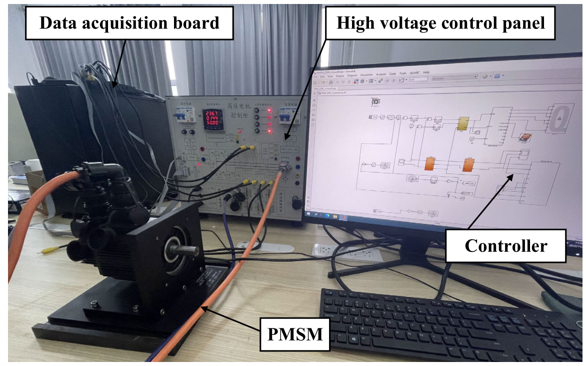

Fig. 8. Experimental setup.

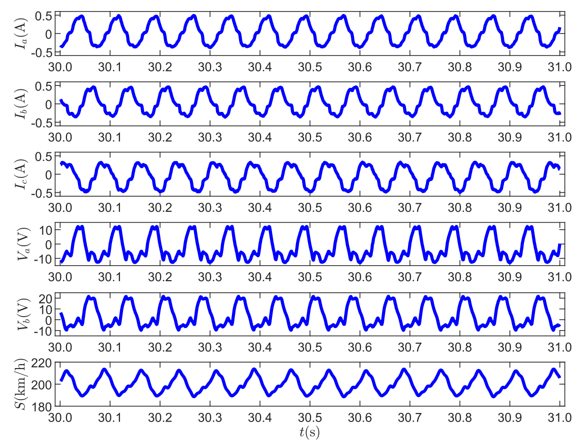

Fig. 9. Free-fault data.

synchronous motor (PMSM) is controlled. The electrical drive system generates a three-phase pulsewidth modulation output to control the current vector [31]. It has been used in practical scenarios [32]. For example, direct torque control and vector control have been used in the traction system of high-speed railways. The structure diagram of the electrical drive system with vector control strategy is shown in Fig. 7. The experimental platform is shown in Fig. 8. Main parameters are presented in Table I. The electrical drive system is equipped with three sensors I_a, I_b, and S for closed-loop control of at least. For FDD purpose, sensors should be used to measure I_a, I_b, I_c, V_a, V_b, and S simultaneously, where I_a, I_b, and I_c stand for the phase currents, V_a and V_b stand for stator voltages, and S is motor speed. The stator currents are transformed into the two synchronously rotating coordinates. The I_d and I_q are used to control the rotor flux and torque, respectively. In the above coordinate transformation process, which can be realized by

$$\begin{cases} I_d = I_1 \cos wt + I_2 \sin wt \\ I_q = -I_1 \sin wt + I_2 \cos wt \end{cases}$$
$$\begin{cases} I_1 = \frac{2}{3}\left(I_a - \frac{1}{2}I_b - \frac{1}{2}I_c\right) \\ I_2 = \frac{2}{3}\left(\frac{\sqrt{3}}{2}I_b - \frac{\sqrt{3}}{2}I_c\right) \end{cases}$$
$$\text{s.t. } I_a + I_b + I_c = 0 \tag{37}$$

where w is the synchronous angular velocity. t denotes the time variable. Many other complex balance relationships should be satisfied in the electrical drive system [31], [33]. The electrical drive systems have complex mathematical mechanisms and external uncertainties disturbances. A number of assumptions were used in building the model [34]: 1) core loss is neglected; the linearity of magnetic circuit is assumed; 2) turbulent flow, high-order space harmonic, and hysteresis loss are neglected; 3) the stator currents are symmetrical sinusoidal; and 4) disturbances or noises obey Gaussian distribution. Six signals, including currents I_a, I_b, I_c, V_a, V_b, and S, are selected in this article. Let

$$z_1 = [I_a, I_b, I_c]^T, \quad z_2 = [V_a, V_b, S]^T. \tag{38}$$

To model the nonlinear, samples are collected from six sensors as shown in Fig. 9. A three-layer neural network is used for forming the RRNCCA method, where the number of hidden layers is 64, the learning rates are 0.01, and the activation function is linear. The FD thresholds $T_{\mathrm{th}_{11}}$, $T_{\mathrm{th}_{12}}$, $T_{\mathrm{th}_{21}}$, and $T_{\mathrm{th}_{22}}$ are obtained via (36).

B. Fault Injection

In this article, three types of fault are considered.

1) An incipient constant bias fault on I_c at the 50.4th s, where the form is $f_1 = 0.025$ A. $f_1 = 0.05$ at the 50.7th s. As shown in Fig. 10, f_1 is unobservable.
2) An incipient constant bias fault on $\{I_a, I_b$, and $I_c\}$ at the 50.4th s, where the fault amplitude is $f_2 = 0.05$ A. As shown in Fig. 11, there are fluctuations in speed.
3) An intermittent fault on S, where the form is $f_3 = 20$ km/h at the moment 50.4–50.7 s. In Fig. 12, f_3 has a significant impact on S. However, through closed-loop control, the other five signals are not affected.

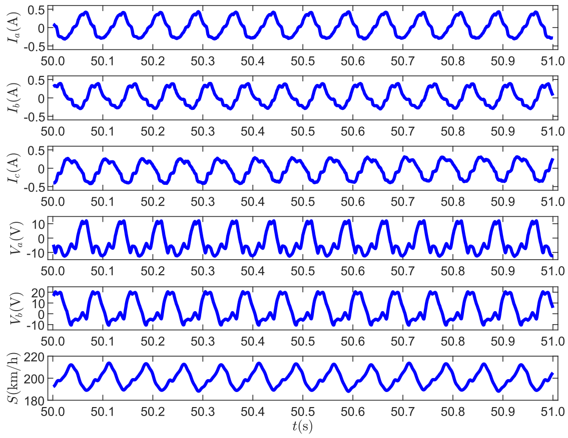

Fig. 10. Influences caused by f_1.

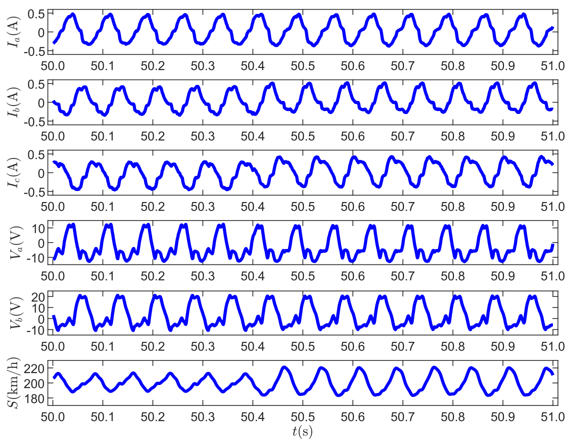

Fig. 11. Influences caused by f_2.

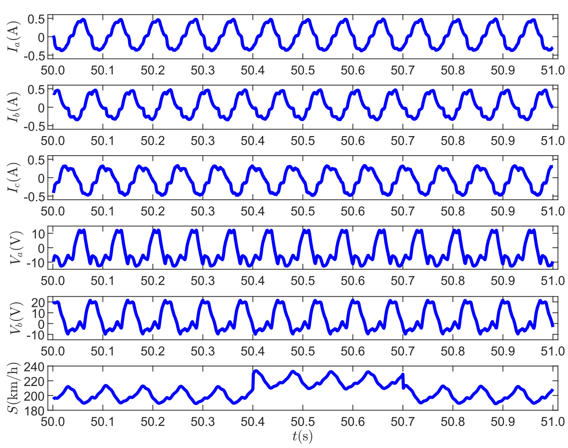

Fig. 12. Influences caused by f_3.

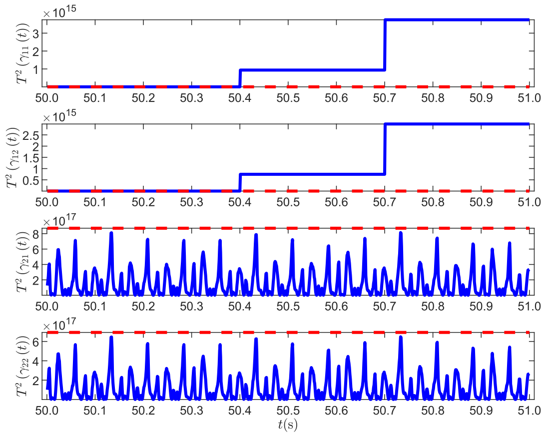

Fig. 13. Detection of f_1 using RRNCCA.

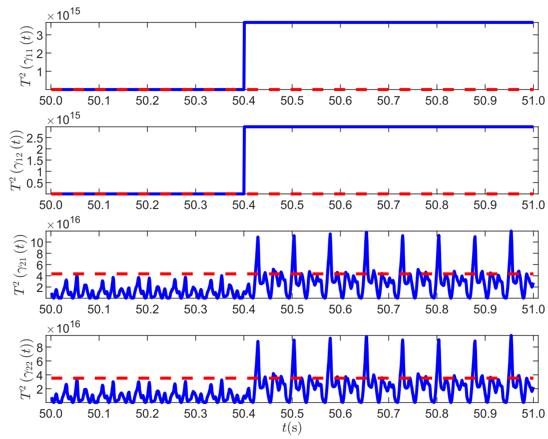

Fig. 14. Detection of f_2 using RRNCCA.

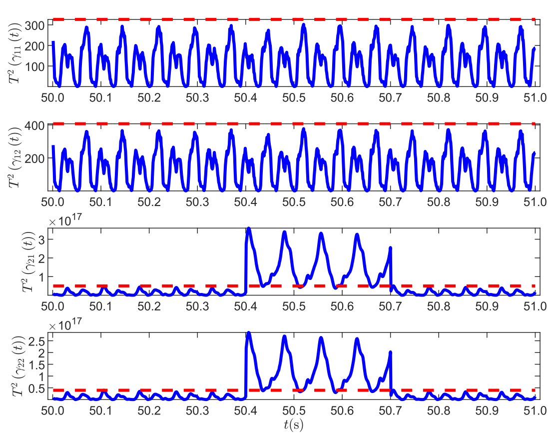

Fig. 15. Detection of f_3 using RRNCCA.

C. RRNCCA-Based FDD Results in Electrical Drive System

To detect f_1, f_2, and f_3, the proposed RRNCCA method is applied. By the use of proposed RRNCCA method, Figs. 13–15 present detection results of f_1, f_2, and f_3, respectively. The blue solid line is test statistic. The red dashed line is threshold.

It is not difficult to see from Fig. 13 that the test statistic quickly exceeds the threshold after the occurrence of faults. In addition, the simulation results are consistent with the theoretical derivations. As shown in Fig. 14, the proposed RRNCCA method successfully detects f_2. As demonstrated in (34) and Fig. 14, the fault is detected in $z_1(k)$. In Fig. 15, $T^2(\gamma_{11})$ and $T^2(\gamma_{12})$ are consistently less than the threshold. After the fault, $T^2(\gamma_{21})$ and $T^2(\gamma_{22})$ quickly exceed the threshold to achieve satisfactory FDD performance. In addition, after the fault disappears, the system quickly adjusts to restore stability.

TABLE II
PERFORMANCE COMPARISON OF THE FOUR METHODS

Methods	Fault	MDRs				FARs				FDD Results
		$T^2\,(\gamma_{11})$	$T^2\,(\gamma_{12})$	$T^2\,(\gamma_{21})$	$T^2\,(\gamma_{22})$	$T^2\,(\gamma_{11})$	$T^2\,(\gamma_{12})$	$T^2\,(\gamma_{21})$	$T^2\,(\gamma_{22})$	
LLGAE	f_1	3.73%	—	—	—	0.13%	—	—	—	—
	f_2	2.31%	—	—	—	0.00%	—	—	—	—
	f_3	4.36%	—	—	—	0.00%	—	—	—	—
CCA	f_1	13.25%	22.87%	—	—	0.50%	0.00%	—	—	**fault in z_1**
	f_2	16.83%	16.83%	—	—	0.28%	0.33%	—	—	—
	f_3	35.48%	26.83%	—	—	0.15%	0.25%	—	—	**fault in z_2**
SsCCA	f_1	4.25%	16.33%	—	—	0.25%	0.37%	—	—	**fault in z_1**
	f_2	8.96%	8.96%	—	—	0.23%	0.21%	—	—	—
	f_3	25.57%	13.86%	—	—	0.09%	0.12%	—	—	**fault in z_2**
RRNCCA	f_1	1.35%	1.35%	98.84%	98.84%	0.03%	0.03%	0.14%	0.14%	**fault in z_1**
	f_2	1.23%	1.23%	82.17%	83.17%	0.09%	0.17%	0.06%	0.13%	**fault in z_1**
	f_3	100.00%	100.00%	4.50%	4.50%	0.08%	0.09%	0.25%	0.25%	**fault in z_2**

Note: bold fonts represent the correct FDD result; "—" means that cannot obtain fault diagnosis results or T^2 test statistics.

To show the FD performance of the RRNCCA, four sets of comparisons with conventional methods (i.e., LLGAE [24], CCA [35], and SsCCA [15]) are made. According to the realization method in [24], the frame of LLGAE is designed. According to the realization method in [15], SsCCA are designed for $z_1(k)$ and $z_2(k)$ faults.

To clearly compare the FD performance, the false alarm rate (FAR) and missed detection rate (MDR) are introduced. The form of FAR and MDR is

$$\mathrm{FAR} = \frac{n_{\text{false}-\text{alarms}}}{n_{\text{no}-\text{fault}}}\%, \quad \mathrm{MDR} = \frac{n_{\text{miss}-\text{detection}}}{n_{\text{fault}}}\% \tag{39}$$

where $n_{\text{no}-\text{fault}}$ represents the total number of fault-free; n_{fault} represents the total fault number; $n_{\text{false}-\text{alarms}}$ represents the total number of false alarms; $n_{\text{miss}-\text{detection}}$ represents the total number of missing detections.

Table II summarizes several important indicators such as FARs, MDRs, and FDD results. The LLGAE has high FD performance when detecting f_1, f_2, and f_3. However, since LLGAE is an unsupervised learning technique, fault diagnosis cannot be achieved [15]. In the FDD process, both CCA and SsCCA methods have $T^2(\gamma_{11}) = T^2(\gamma_{12})$ cases. At this time, CCA and SsCCA cannot diagnose faults.

V. CONCLUSION

In this study, an RRNCCA-based FDD framework is proposed. It can parameterize the correlated representations of nonlinear electrical drive systems. It minimizes the uncertainty of the residual signal by extracting the maximum correlation hidden in the nonlinear relationship. Through theoretical reasoning, the proposed RRNCCA method can perform FDD. The realization method of RRNCCA is introduced in detail. An experimental platform for electrical drive systems is introduced to validate the FDD performance of the RRNCCA method. As it turns out, this scheme also provides the best FDD performance. The significant value of this method is that a reversible nonlinear CCA framework based on RRN is constructed. The future effort is committed to realizing the application of FDD in dynamic nonlinear systems.

APPENDIX A
LINEAR AND NONLINEAR OPERATORS

The linear and nonlinear operators can be defined as

$$\begin{aligned}&\text{linear operator } A : (P \to Q),\ A(p) = \Phi p = q\\ &\text{nonlinear operator } A : (P \to Q),\ A(p) = q\end{aligned} \tag{A.1}$$

holds for any vector $p \in P$ and any scalar $\Phi \in R$. Here, q is the basis spanning the vector space Q. Therefore, the linear and nonlinear operators can be described as $A(p) = q$ in a unified manner. Considering two operators ($A : P \to Q$ and $B : Q \to V$), the cascade connection of two operators is denoted as

$$(B \circ A)p = B(A(p)). \tag{A.2}$$

APPENDIX B
DETAILS (16)

$$\begin{aligned}&\theta : z_1(k) \to z_2(k)\\ &\frac{\partial \theta z_1(k)}{\partial z_1^T(k)} = \frac{\partial z_2(k)}{\partial z_1^T(k)}.\end{aligned} \tag{B.1}$$

Equation (B.1) combined with (4), obtained

$$\frac{\partial \theta z_1(k)}{\partial z_1^T(k)} = \frac{\partial \begin{bmatrix} z_{21}(k) \\ z_{22}(k) \end{bmatrix}}{\partial \begin{bmatrix} z_{11}(k) \\ z_{11}(k) \end{bmatrix}^T} = \begin{bmatrix} I & \dfrac{\partial F}{\partial z_{12}^T(k)} \\ -\dfrac{\partial G}{\partial z_{11}^T(k)} & I - \dfrac{\partial G}{\partial F} \frac{\partial F}{\partial z_{12}^T(k)} \end{bmatrix} \tag{B.2}$$

where $(\partial G/\partial F) = (\partial G/(\partial z_{11}^T(k)))$. Therefore,

$$\begin{aligned}\frac{\partial \theta z_1(k)}{\partial z_1^T(k)} &= \begin{bmatrix} I & \dfrac{\partial F}{\partial z_{12}^T(k)} \\ -\frac{\partial G}{\partial z_{11}^T(k)} & I - \dfrac{\partial G}{\partial z_{11}^T(k)} \frac{\partial F}{\partial z_{12}^T(k)} \end{bmatrix}\\ &= \begin{bmatrix} I & 0 \\ -\dfrac{\partial G}{\partial z_{11}^T(k)} & I \end{bmatrix} \begin{bmatrix} I & \dfrac{\partial F}{\partial z_{12}^T(k)} \\ 0 & I \end{bmatrix}.\end{aligned} \tag{B.3}$$

Therefore,

$$\det\left(\frac{\partial \theta z_1(k)}{\partial z_1{}^T(k)}\right) = \begin{vmatrix} I & 0 \\ -\dfrac{\partial G}{\partial z_{11}^T(k)} & I \end{vmatrix} \begin{vmatrix} I & \dfrac{\partial F}{\partial z_{12}^T(k)} \\ 0 & I \end{vmatrix} = 1. \tag{B.4}$$

REFERENCES

[1] H. Chen, Z. Liu, C. Alippi, B. Huang, and D. Liu, "Explainable intelligent fault diagnosis for nonlinear dynamic systems: From unsupervised to supervised learning," *IEEE Trans. Neural Netw. Learn. Syst.*, pp. 1–14, Sep. 2022, doi: 10.1109/TNNLS.2022.3201511.

[2] J. Dong and G.-H. Yang, "Reliable state feedback control of T–S fuzzy systems with sensor faults," *IEEE Trans. Fuzzy Syst.*, vol. 23, no. 2, pp. 421–433, Apr. 2015.

[3] S. Yang, D. Xiang, A. Bryant, P. Mawby, L. Ran, and P. Tavner, "Condition monitoring for device reliability in power electronic converters: A review," *IEEE Trans. Power Electron.*, vol. 25, no. 11, pp. 2734–2752, Nov. 2010.

[4] Z. Mao, G. Tao, B. Jiang, and X.-G. Yan, "Adaptive compensation of traction system actuator failures for high-speed trains," *IEEE Trans. Intell. Transp. Syst.*, vol. 18, no. 11, pp. 2950–2963, Nov. 2017.

[5] C. Cheng, W. Wang, H. Chen, B. Zhang, J. Shao, and W. Teng, "Enhanced fault diagnosis using broad learning for traction systems in high-speed trains," *IEEE Trans. Power Electron.*, vol. 36, no. 7, pp. 7461–7469, Jul. 2021.

[6] C. Cheng, X. Qiao, B. Zhang, H. Luo, Y. Zhou, and H. Chen, "Multiblock dynamic slow feature analysis-based system monitoring for electrical drives of high-speed trains," *IEEE Trans. Instrum. Meas.*, vol. 70, pp. 1–10, 2021.

[7] X. Kong, Z. Yang, J. Luo, H. Li, and X. Yang, "Extraction of reduced fault subspace based on KDICA and its application in fault diagnosis," *IEEE Trans. Instrum. Meas.*, vol. 71, pp. 1–12, 2022.

[8] C. Cheng, W. Wang, X. Meng, H. Shao, and H. Chen, "Sigma-mixed unscented Kalman filter-based fault detection for traction systems in high-speed trains," *Chin. J. Electron.*, vol. 32, no. 5, pp. 982–991, Sep. 2023.

[9] S. Shao, R. Yan, Y. Lu, P. Wang, and R. X. Gao, "DCNN-based multi-signal induction motor fault diagnosis," *IEEE Trans. Instrum. Meas.*, vol. 69, no. 6, pp. 2658–2669, Jun. 2020.

[10] C. Cheng, W. Wang, G. Ran, and H. Chen, "Data-driven designs of fault identification via collaborative deep learning for traction systems in high-speed trains," *IEEE Trans. Transport. Electrific.*, vol. 8, no. 2, pp. 1748–1757, Jun. 2022.

[11] H. Chen and B. Jiang, "A review of fault detection and diagnosis for the traction system in high-speed trains," *IEEE Trans. Intell. Transp. Syst.*, vol. 21, no. 2, pp. 450–465, Feb. 2020.

[12] H. Chen, B. Jiang, S. X. Ding, and B. Huang, "Data-driven fault diagnosis for traction systems in high-speed trains: A survey, challenges, and perspectives," *IEEE Trans. Intell. Transp. Syst.*, vol. 23, no. 3, pp. 1700–1716, Mar. 2022.

[13] P. Odiowei and Y. Cao, "Nonlinear dynamic process monitoring using canonical variate analysis and kernel density estimations," in *Proc. 10th Int. Symp. Process Syst. Eng., A* (Computer Aided Chemical Engineering), vol. 27, R. M. de Brito Alves, C. A. O. do Nascimento, and E. C. Biscaia, Eds. Amsterdam, The Netherlands: Elsevier, 2009, pp. 1557–1562.

[14] J. Li, D. Ding, and F. Tsung, "Directional PCA for fast detection and accurate diagnosis: A unified framework," *IEEE Trans. Cybern.*, vol. 52, no. 11, pp. 11362–11372, Nov. 2022.

[15] H. Chen, Z. Chen, Z. Chai, B. Jiang, and B. Huang, "A single-side neural network-aided canonical correlation analysis with applications to fault diagnosis," *IEEE Trans. Cybern.*, vol. 52, no. 9, pp. 9454–9466, Sep. 2022.

[16] Z. Chen, X. Li, X. Shaolong, T. Peng, C. Yang, and W. Gui, "Feature correlation-based ground fault diagnosis method for main circuit of traction system," *Acta Automatica Sinica*, vol. 47, no. 7, pp. 1516–1529, 2021.

[17] Z. Chen, K. Liang, S. X. Ding, C. Yang, T. Peng, and X. Yuan, "A comparative study of deep neural network-aided canonical correlation analysis-based process monitoring and fault detection methods," *IEEE Trans. Neural Netw. Learn. Syst.*, vol. 33, no. 11, pp. 6158–6172, Nov. 2022.

[18] H. Knutsson, M. Borga, and T. Landelius, "Learning multidimensional signal processing," in *Proc. 14th Int. Conf. Pattern Recognit.*, Aug. 1998, pp. 1416–1420.

[19] Z. Chen, S. X. Ding, T. Peng, C. Yang, and W. Gui, "Fault detection for non-Gaussian processes using generalized canonical correlation analysis and randomized algorithms," *IEEE Trans. Ind. Electron.*, vol. 65, no. 2, pp. 1559–1567, Feb. 2018.

[20] C. L. P. Chen and Z. Liu, "Broad learning system: An effective and efficient incremental learning system without the need for deep architecture," *IEEE Trans. Neural Netw. Learn. Syst.*, vol. 29, no. 1, pp. 10–24, Jan. 2018.

[21] P. L. Lai and C. Fyfe, "A neural implementation of canonical correlation analysis," *Neural Netw.*, vol. 12, no. 10, pp. 1391–1397, Dec. 1999.

[22] Q. Jiang and X. Yan, "Learning deep correlated representations for nonlinear process monitoring," *IEEE Trans. Ind. Informat.*, vol. 15, no. 12, pp. 6200–6209, Dec. 2019.

[23] H. Chen, Z. Chai, B. Jiang, and B. Huang, "Data-driven fault detection for dynamic systems with performance degradation: A unified transfer learning framework," *IEEE Trans. Instrum. Meas.*, vol. 70, pp. 1–12, 2021.

[24] C. Cheng, Y. Ju, S. Xu, Y. Lv, and H. Chen, "Local linear generalized autoencoder-based incipient fault detection for electrical drive systems of high-speed trains," *IEEE Trans. Intell. Transp. Syst.*, vol. 24, no. 11, pp. 12422–12430, Jun. 2023.

[25] A. N. Gomez, M. Ren, R. Urtasun, and R. B. Grosse, "The reversible residual network: Backpropagation without storing activations," in *Proc. Adv. Neural Inf. Process. Syst.*, vol. 30, 2017, pp. 2211–2221.

[26] D. R. Hardoon, S. Szedmak, and J. Shawe-Taylor, "Canonical correlation analysis: An overview with application to learning methods," *Neural Comput.*, vol. 16, no. 12, pp. 2639–2664, Dec. 2004.

[27] C. Chatfield, *Introduction to Multivariate Analysis*. Evanston, IL, USA: Routledge, 2018.

[28] L. Dinh, D. Krueger, and Y. Bengio, "NICE: Non-linear independent components estimation," 2014, *arXiv:1410.8516*.

[29] H. Chen and B. Huang, "Explainable fault diagnosis using invertible neural networks—Part I: A left manifold-based solution," *TechRxiv*, Oct. 2023, doi: 10.36227/techrxiv.24314065.v1.

[30] H. Hotelling, "Relations between two sets of variates," in *Breakthroughs Statistics: Methodology Distribution*. New York, NY, USA: Springer, 1992, pp. 162–190.

[31] J. W. Finch and D. Giaouris, "Controlled AC electrical drives," *IEEE Trans. Ind. Electron.*, vol. 55, no. 2, pp. 481–491, Jan. 2008.

[32] G. S. Buja and M. P. Kazmierkowski, "Direct torque control of PWM inverter-fed AC motors—A survey," *IEEE Trans. Ind. Electron.*, vol. 51, no. 4, pp. 744–757, Aug. 2004.

[33] J. Zhang, J. Zhao, D. Zhou, and C. Huang, "High-performance fault diagnosis in PWM voltage-source inverters for vector-controlled induction motor drives," *IEEE Trans. Power Electron.*, vol. 29, no. 11, pp. 6087–6099, Nov. 2014.

[34] T. A. Najafabadi, F. R. Salmasi, and P. Jabehdar-Maralani, "Detection and isolation of speed-, DC-link voltage-, and current-sensor faults based on an adaptive observer in induction-motor drives," *IEEE Trans. Ind. Electron.*, vol. 58, no. 5, pp. 1662–1672, May 2011.

[35] S. X. Ding, *Data-Driven Design of Fault Diagnosis and Fault-Tolerant Control Systems*. London, U.K.: Springer-Verlag, 2014.

Shenquan Wang received the Ph.D. degree in control science and engineering from Northeastern University, Shenyang, China, in 2014.

From November 2014 to July 2017, he was a Post-Doctoral Research Associate with the State Key Laboratory of Management and Control for Complex Systems, Institute of Automation, Chinese Academy of Sciences, Beijing, China. From 2021 to 2022, he was an Academic Visitor with the Department of Automation, Tsinghua University, Beijing. He is currently a Professor with the College of Electrical and Electronic Engineering, Changchun University of Technology, Changchun, China. His main research interests include robust stability theory, adaptive/distributed control, and complex systems security and reliability.

Yunfei Ju (Graduate Student Member, IEEE) received the B.Eng. and M.Eng. degrees from the School of Computer Science and Engineering, Changchun University of Technology, Changchun, China, in 2021 and 2023, respectively, where he is currently pursuing the Ph.D. degree with the School of Mechanical and Electrical Engineering.

He applied for the doctoral programs of study in 2023. His main research interests include multivariate statistical analysis, manifold learning, neural network, and their applications to the complex system fault detection and diagnosis.

Caixin Fu received the bachelor's and master's degrees from the School of Communication Engineering, Jilin University, Changchun, China, in 2011 and 2014, respectively. She is currently pursuing the Ph.D. degree with the School of Mechanical and Electrical Engineering, Changchun University of Technology, Changchun.

From 2014 to 2023, she worked with CRRC Changchun Railway Vehicles Company Ltd., Changchun. Her research interests are intelligent electromechanical equipment and control.

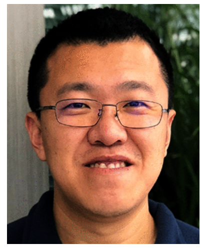

Pu Xie received the Ph.D. degree from the Department of Mechanical Engineering, Tsinghua University, Beijing, China, in 2016.

After graduation, he joined CRRC Changchun Railway Vehicles Company, Ltd., where he conducted experimental research on structural fatigue and crack behavior using the MTS system. He is currently a Visiting Post-Doctoral Scholar with the Department of Aeronautics and Astronautics, Stanford University, Stanford, CA, USA. His research interests include developing and implementing advanced testing and diagnostic methods that enhance the safety and reliability of mechanical systems, as well as developing multiphysics analytical methods for solving complex problems.

Chao Cheng (Member, IEEE) received the M.Eng. and Ph.D. degrees from Jilin University, Changchun, China, in 2011 and 2014, respectively.

He has been a Post-Doctoral Fellow of process control engineering with the Department of Automation, Tsinghua University, Beijing, China, since 2018. He has also been a Post-Doctoral Fellow with the National Engineering Laboratory, CRRC Changchun Railway Vehicles Company Ltd., Changchun, since 2018. He is currently a Professor with the Changchun University of Technology, Changchun. His research interests include dynamic system fault diagnosis and predictive maintenance, wireless sensor networks, artificial intelligence, and data-driven method.